Optimization of electric bus scheduling considering stochastic volatilities in trip travel time and energy consumption

(article starts on next page)

COMPUTER-AIDED CIVIL AND INFRASTRUCTURE ENGINEERING — WILEY

Optimization of electric bus scheduling considering stochastic volatilities in trip travel time and energy consumption

Yiming Bie[1] | Jinhua Ji[1] | Xiangyu Wang[2,3] | Xiaobo Qu[4]

[1] School of Transportation, Jilin University, Changchun, China

[2] School of Civil Engineering and Architecture, East China Jiaotong University, Nanchang, China

[3] School of Design and Built Environment, Curtin University, Perth, Australia

[4] Department of Architecture and Civil Engineering, Chalmers University of Technology, Gothenburg, Sweden

Correspondence
Xiangyu Wang, School of Civil Engineering and Architecture, East China Jiaotong University, Nanchang, 330013, China.
Email: Xiangyu.Wang@curtin.edu.au

Abstract

This paper develops a vehicle scheduling method for the electric bus (EB) route considering stochastic volatilities in trip travel time and energy consumption. First, a model for estimating the trip energy consumption is proposed based on field-collected data, and the probability distribution function of trip energy consumption considering the stochastic volatility is determined. Second, we propose the charging strategy to recharge buses during their idle times. The impacts of stochastic volatilities on the departure time, the idle time, the battery state of charge, and the energy consumption of each trip are analyzed. Third, an optimization model is built with the objectives of minimizing the expectation of delays in trip departure times, the summation of energy consumption expectations, and bus procurement costs. Finally, a real bus route is taken as an example to validate the proposed method. Results show that reasonable idle times can be generated by optimizing the scheduling plan, and it is helpful to stop the accumulation of stochastic volatilities. Collaboratively optimizing vehicle scheduling and charging plans can reduce the EB fleet and delay times while meeting the route operation needs.

1 | INTRODUCTION

1.1 | Background

With the features of zero-emissions, low noise level, and high driving stability, electric buses (EBs) have evident superiorities in reducing air pollution emissions and saving operation costs of transit corporations. Therefore, the deployment of EBs has been promoted and continuously expanded recently. According to research conducted by

Bloomberg New Energy Finance Electric, it is estimated that the number of EBs worldwide will reach 1.2 million by 2025, which accounts for 47% of all buses (Chediak, 2018). Until the end of 2019, China has 0.69 million buses in urban areas including 0.32 million EBs, which accounts for 46.8% of all buses. Besides, the number of EBs in China is expected to rise to approximately 0.4 million by the end of 2020. Over the past five years, the number of EBs in Europe has increased from around 200 to 2200 vehicles, according to a report from Busworld (Millikin, 2019). By the end

of 2020, there will be 220 EBs operate in the Gothenburg area, Sweden (Weekes, 2020). Bogotá, the capital city of Colombian, will give the city the largest EB fleet in Latin America (Dzikiy, 2019). In Canada, the cities of Laval and Montreal plan to purchase only EBs by 2023 and 2025 (Montreal Gazette, 2018).

In addition to the aforementioned advantages, EBs have limitations such as shorter driving range and longer charging time, compared with fuel buses (N. Jiang & Xie, 2014). Hence, charging strategies for EBs are required to maintain their daily operations when making scheduling plans. The selection of charging strategies will affect not only the number of buses available to be deployed on a transit route but also energy consumptions and battery cycle life. The normal charging strategy used currently is to recharge the battery when it is about exhausted until fully charged. However, this high depth of discharge (DOD) would severely jeopardize battery life. To mitigate this depreciation, keeping the battery working around a medium state of charge (SOC) level is the most beneficial method, but the bus fleet size should be amplified accordingly. Considering these battery features, it is a wise option for us to take full use of idle times, which occur during nonpeak hours in daily operation, to recharge EBs. This will increase the driving range, reduce energy consumptions, avoid the enlargement of bus fleet size caused by demands of recharging while maintaining SOC around a reasonable level, effectively prolonging the battery cycle life. The durations and number of idle times of each bus during all-day operations are directly determined by the trips that each bus is required to serve, which are arranged by vehicle scheduling. Therefore, the optimization of vehicle scheduling plans is crucial for the improvement of the operational efficiency of an EB route.

Trip travel time is a significant factor to be considered in the vehicle scheduling problem (VSP). The stochastic volatility occurs in trip travel time under the influences of signalized intersections and random passenger demands at bus stations. This will result in the actual departure times of some trips being later than the scheduled departure times, and the delay can propagate through continuous trips served by the same bus, reducing the reliability of transit service.

Meanwhile, energy consumption is another factor that needs special consideration in the VSP of EBs. It is revealed by the analysis of actual data that energy consumptions of EBs on routes have stochastic volatility as well. Differences in energy consumption even exist on trips with the same travel time and SOC at departure terminals. This stochastic volatility makes it difficult to estimate energy consumption accurately. Inaccurate estimation would result in the service interruptions caused by battery exhaustion of buses running on routes. Thus, it is fundamental to accu-

rately estimate energy consumptions of EBs for the VSP optimization so as to avoid service interruptions, generate more intelligent charging plans, and improve the operation reliability of transit routes.

From the above, it is concluded that conventional vehicle scheduling methods are not applicable to EBs. When developing vehicle scheduling plans for EB routes, the influences of recharging behaviors, limited driving range, and stochastic volatilities in their trip travel times and energy consumptions should be taken into account.

1.2 | Literature review

Most current research efforts in VSPs concentrate on conventional fuel buses, such as the scheduling problem overview (Adler, 2014; Bunte & Kliewer, 2009; Ceder, 2002; Laporte, 2009; Meng & Qu, 2013; H. Wang & Shen, 2007; S. Wang et al., 2018), the multiple depot VSPs (Hadjar et al., 2006), vehicle scheduling with multi-vehicle types (Ceder, 2011), vehicle and crew scheduling problem (Amberg et al., 2019; Kliewer et al., 2012), integrated approach to timetabling and vehicle scheduling (Ibarra-Rojas et al., 2014; Schmid & Ehmke, 2015), dynamic control method (Bie et al., 2020; Khan et al., 2019; M. Li et al., 2011; Xie & Jiang, 2016), reliability of trip times (Liu et al., 2013; Naumann et al., 2011; Shen et al., 2017), and other intelligent transportation systems (Adeli & Ghosh-Dastidar, 2004; Adeli & Jiang, 2009; Gao et al., 2020, 2021; Ghosh-Dastidar & Adeli, 2006; X. Jiang & Adeli, 2003; S. Wang, Wei, et al., 2019; Xu et al., 2021).

With the recent promotion and deployment of EBs, more studies about EBs have been conducted, mainly focused on the optimization of charging infrastructure (An, 2020; Y. He et al., 2019; Qu et al., 2020; Rogge et al., 2018; X. Zhang et al., 2018; D. Zhao, Li, et al., 2019), lifecycle costs evaluation (Fusco et al., 2013; Lajunen, 2018; J. Q. Li, 2016; Ritari et al., 2020) and the EB fleet transition problem (Logan et al., 2020; Pelletier et al., 2019; Teoh et al., 2018), dynamic control of EBs (Al-Ogaili et al., 2020; H. He et al., 2018; Wang et al., 2019; L. Zhang et al., 2020), and so forth. For VSP of EBs, studies can be categorized into the following two groups according to power types of buses on the routes:

(i) Vehicle scheduling of pure EBs

J. Q. Li (2014) developed a column-generation-based algorithm to solve the vehicle scheduling model for EBs with either battery swapping or fast charging at a battery station. Wen et al. (2016) presented a mixed integer programming formulation as well as an adaptive large neighborhood search heuristic algorithm for VSP of pure

EBs. The proposed heuristic algorithm could provide good solutions to large instances and optimal or near-optimal solutions to small instances. van Kooten Niekerk et al. (2017) took into consideration the impact of actual electricity price and the battery depreciation cost on VSP of EBs. Three kinds of vehicle scheduling models were established and solved by integer linear programming and column generation. Guo et al. (2019) proposed a genetic algorithm-based column generation approach for VSP of a class of multi-depot EBs.

Tang et al. (2019) presented robust scheduling strategies of EBs to tackle the challenge brought by the stochasticity of urban traffic conditions and introduced a buffer distance strategy into the static model to deal with the adverse effects of travel time randomness. Teng et al. (2020) focused on the bus timetabling and VSP for EBs and developed a multi-objective optimization model for a single bus line. With explicit consideration of differences in driving range, recharging duration, and energy consumption of EBs with multiple vehicle types, Yao et al. (2020) established an optimization model with the minimum annual total scheduling cost. J. Wang et al. (2020) proposed an optimal scheduling method based on dynamic programming to minimize the battery replacement cost during the entire service life of EB fleets.

Trip energy consumption estimation is one important part of the EB scheduling. Basma et al. (2020) proposed a comprehensive energy estimation model to emulate the propulsion load, heating ventilating and air conditioning system, and auxiliaries necessary for the bus operation. El-Taweel et al. (2020) developed a model to calculate the EB energy consumption by generating a set of speed profiles using the basic information of the bus trip: Trip time, trip length, and distances between successive bus stops. X. Zhao, Ye, et al. (2020) and X. Zhao, Zhao, et al. (2020) evaluated energy consumption, driving range, and equivalent emissions for specific cities or areas using the construction of a real-world driving cycle. Al-Ogaili et al. (2020) developed a longitudinal dynamic model with a spatial version of a digital elevation model to determine the energy demand of a large-scale battery EB network. Additionally, they also assessed two charging protocols: Opportunity charging and overnight charging, according to the operating environments of EBs.

ii Vehicle scheduling of mixed buses

Here "mixed buses" means the combination of pure EBs and hybrid buses. Rinaldi et al. (2018) studied the problem of optimally determining the sequence of electric and hybrid buses departing from a multi-line bus terminal, considering both service and energy constraints. The problem was formulated as a mixed integer linear program, with the objective of minimizing the total operational cost

for bus lines. Rinaldi et al. (2020) also addressed the problem of optimal scheduling of a mixed fleet of electric and hybrid in the same way. Test results based on a real-life scenario showed that the proposed method could significantly reduce operating costs.

L. Li et al. (2019) developed a formulation for the multiple depot VSP with multiple vehicle types, including EBs, under range, and refueling constraints. Sivagnanam et al. (2020) introduced an integer program for optimal discrete-time scheduling model to minimize fuel and electricity use by assigning vehicles to transit trips and scheduling them for charging while serving an existing fixed-route transit schedule. Picarelli et al. (2020) presented a mixed-integer linear programming model for the mixed bus fleet scheduling problem and implemented a time-based decomposition framework. This method could provide near-optimal solutions that explicitly considered the energy constraints arising from EB operations while establishing an advantageous trade-off between delaying trips to implement quick charging of EBs. Zhou et al. (2020) established a multi-objective bi-level programming model to collaboratively optimize the vehicle scheduling and charging scheduling of the mixed bus fleet with electric and traditional buses and solved with an integrated heuristic algorithm.

However, the aforementioned studies did not consider the impacts of stochastic volatilities in trip travel times and energy consumptions on VSP of EBs, and most of them assumed that energy consumption rates of EBs during operation remain constant. Actually, energy consumptions are affected by multiple factors such as trip travel time, battery SOC at the departure time, and temperature. Besides, the energy consumption of the previous trip will influence battery SOC at the departure time of the next trip along with its energy consumption, which makes the energy consumption rate fluctuate during all-day operation time instead of maintaining a constant value. Hence, taking the stochastic volatility into consideration will lead to a more accurate estimation of energy consumptions of EBs on routes, and consequently generating more reliable vehicle scheduling and charging plans.

1.3 | Contributions

This paper develops a vehicle scheduling method for the EB route with regards to stochastic volatilities of trip travel time and energy consumption. The contributions of this study include: (i) Developing a method to determine the probability distribution function (PDF) for trip energy consumption. The PDF is utilized to describe the stochastic volatility in energy consumption and help improve the reliability of the optimization model; (ii) proposing a strategy of leveraging idle time to recharge EBs and analyzing influences caused by the stochastic volatilities in trip
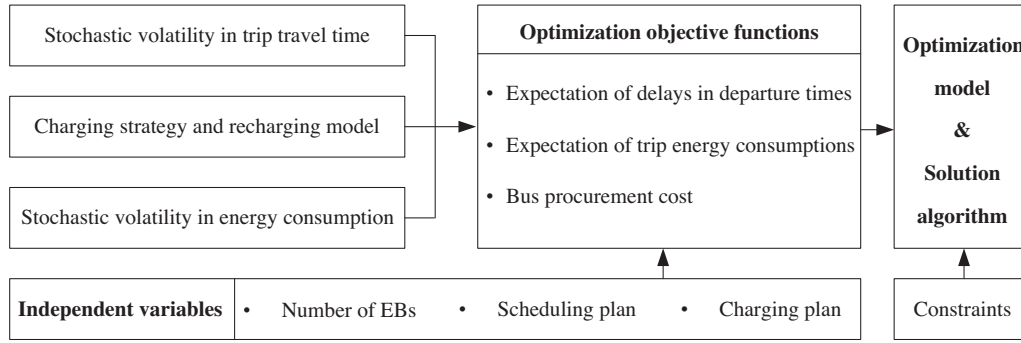
FIGURE 1   The overall structure of the methodology

travel times and energy consumptions on the departure time, the idle time, and the energy consumption of each trip. On this basis, with the objectives of minimizing the expectation of delays in departure times, the summation of energy consumption expectations, the bus procurement costs, optimization methods of vehicle scheduling, and charging plans are obtained for the EB fleet in multiple periods per day.

The remainder of this paper is organized as follows. Section 2 provides the expression methods of stochastic volatilities in trip travel time and energy consumption and establishes a multi-objective optimization model for VSP of EBs. Section 3 displays a numerical example based on a real EB route. Finally, some concluding remarks and possible future works are given in Section 4.

2 | METHODOLOGY

Under the influences of stochastic volatilities in trip travel time and energy consumption, the expected optimization plan would reduce the delay in trip departure times and energy consumptions. However, such a plan would require a larger fleet size and increase bus procurement costs, which do not comply with the expectation of the transit corporation. Therefore, this paper developed a multi-objective optimization model addressing the VSP for an electric transit route, with the objectives of minimizing the expectation of delays in trip departure times, the summation of energy consumption expectations, and bus procurement costs so as to optimize the trip sets and charging plans for each EB during daily operation time, collaboratively. Figure 1 displays the structure of the methodology. Sections 2.1 to 2.3 display stochastic volatilities and charging models. Section 2.4 presents the calculation methods for the optimization objectives, and Section 2.5 introduces the solution algorithm.

Let o be the running direction of an EB bus route. $o = 1$ refers to the inbound trip, while $o = 2$ refers to the outbound trip. This route consists of M stops. Battery charg-

ing devices are installed at station 1 and station M to provide charging services for EBs. K EBs can be deployed at most on this route under the limitation of the procurement budget of a transit corporation. Let k be the serial number of each EB, $k = 1, 2, \dots, K$. The operation time per day is divided into Q periods, and let q represent each period, $q = 1, 2, \dots, Q$. One bus running from starting station 1 to terminal station M (inbound) or from station M to station 1 (outbound) is defined as one complete trip. An inbound trip is represented by i, $i = 1, 2, \dots, N^1$, and an outbound trip by j, $j = 1, 2, \dots, N^2$. N^1 and N^2 are the total numbers of inbound and outbound trips during all-day operation time.

The objective of this research is to determine the set of trips run by EB k, denoted by X_k. If EB k runs the outbound trip j after serving the inbound trip i, then $x_{kij} = 1$; otherwise, $x_{kij} = 0$. Similarly, if EB k runs the inbound trip i after running the outbound trip j, then $x'_{kji} = 1$; otherwise, $x'_{kji} = 0$. Specifically, x_{k0j} represents that the service of EB k starts from the outbound trip j, and x_{ki0} represents that the service of EB k ends after the inbound trip i. For instance, $x_{302} = 1$ indicates that the first task of EB 3 is to run the second outbound trip; $x_{390} = 1$ indicates that EB 3 ends the daily operation after finishing the ninth inbound trip.

2.1 | Stochastic volatility in trip travel time

Trip travel time is a major element in the static vehicle scheduling process (Yu et al., 2018). However, it is affected by multiple factors including traffic conditions, signalized intersection timing schemes, and passenger demands at bus stations, which cause the stochastic volatilities in trip travel times. Thus, in this paper, the actual trip travel time is denoted by a discrete variable of which the value fluctuates within a certain interval with 1-min step and fits a PDF, namely, $t_i \in [t_i^{\min}, t_i^{\max}]$ for the actual travel time of inbound trip i and $t_j \in [t_j^{\min}, t_j^{\max}]$ for the actual travel time of outbound trip j, min. Here, $t_i^{\min}, t_i^{\max}, t_j^{\min}$ and $t_j^{\max}$

are the minimum and maximum actual travel times of trips i and j, respectively. The number of possible time points of the trip i is represented by G_i and $G_i = t_i^{\max} - t_i^{\min} + 1$. Hence, the first possible travel time of trip i is $t_i^{\min}$. The g_i-th possible travel time is $(t_i^{\min} + g_i - 1)$ and its probability can be denoted as $p(t_i = t_i^{g_i}), 1 \leq g_i \leq G_i$. In a similar way, the probability of the g_j-th possible travel time of trip j is $p(t_j = t_j^{g_j}), 1 \leq g_j \leq G_j$ and $G_j = t_j^{\max} - t_j^{\min} + 1$.

With the stochastic volatilities in trip travel times, the actual end time of trip iT_{ki}^a is also stochastic,

$$T_{ki}^a = T_{ki}^d + t_i, \quad T_{ki}^a \in \left[T_{ki}^{a,\min}, T_{ki}^{a,\max} \right] \quad (1)$$

where T_{ki}^d is the actual departure time of trip i run by EB k; $T_{ki}^{a,\min} = T_{ki}^d + t_i^{\min}$ and $T_{ki}^{a,\max} = T_{ki}^d + t_i^{\max}$ are the minimum and maximum end times of trip i. Obviously, the probability that trip i would end at the g_i-th time point is equal to $p(t_i = t_i^{g_i})$, and T_{ki}^a can also take G_i possible values, denoted by $p(T_{ki}^a = T_{ki}^{a,g_i}) = p(t_i = t_i^{g_i})$.

The stochastic T_{ki}^a leads to the uncertainty in the feasibility of EB k running two trips. Let $i\Theta j$ represent the time feasibility that trip j can be served after trip i by EB k. The probability of time feasibility $P_k(i\Theta j)$ can be calculated by

$$P_k(i\Theta j) = p\left(T_{ki}^a \leq T_{kj}^D \right) = \sum_{g_i=1}^{\tau_1} p\left(T_{ki}^a = T_{ki}^{a,g_i} \right) \quad (2)$$

where T_{kj}^D is the scheduled departure time of trip j regulated by timetable; τ_1 is the serial number that can be potentially taken by T_{ki}^a when $T_{ki}^a = T_{kj}^D, 1 \leq \tau_1 \leq G_i$.

When $T_{kj}^D \geq T_{ki}^{a,\max}$, $P_k(i\Theta j) = 1$, indicating that EB k can definitely depart punctually. When $T_{ki}^{a,\min} \leq T_{kj}^D < T_{ki}^{a,\max}$, $0 < P_k(i\Theta j) < 1$, under which circumstance that EB k might depart later than the scheduled time but is still feasible. It is beneficial for making more reliable scheduling plans with a relatively smaller bus fleet size. Similarly, the feasibility that trip j and another trip i can be served by EB k is $P_k(j\Theta i) = p(T_{kj}^a \leq T_{ki}^D)$.

2.2 | Charging strategy and recharging model

Due to the limited driving range of EBs, it is required to seize appropriate opportunities for recharging during operation time. The selection of charging strategies affects not only the number of buses available to be deployed on a transit route but also the battery cycle life. The most effective way to alleviate the battery life depreciation proved by the experiments conducted by Jana et al. (2019) is to keep a battery working around medium SOC level (around

50%). The thermodynamic performance of batteries shows significant degradation at a high SOC level, while the dynamic performance fades sharply at a low SOC level. Therefore, to mitigate the depreciation and avoid over-discharge, a safety threshold $[\lambda_2, \lambda_1]$ is set for battery SOC during scheduling, where λ_1 and λ_2 are the upper and lower bound of SOC (%), respectively.

There are high dispatching frequencies for a bus route during peak hours. Charging buses during this period would reduce the number of buses available for operation. However, passenger demand drops during nonpeak hours, and some EBs are under the idle state, waiting for running the next trip at terminals. Taking full utilization of idle times to recharge buses would increase the battery SOC, maintaining it within the interval $[\lambda_2, \lambda_1]$ and extending the driving range.

Let a binary variable γ_{kij} indicate whether EB k is under the idle state and η is a constant, min. When $T_{kj}^D - T_{ki}^a \geq \eta$, EB k is identified as being in the idle state after ending trip i, which is expressed as $\gamma_{kij} = 1$; otherwise, $\gamma_{kij} = 0$, which means that EB k should serve trips i and j continuously.

The recharging model is demonstrated here with the inbound trip i as an example. EBs will get recharged in the idle time and battery SOC cannot be higher than λ_1 after recharging. The recharging time for EB k after ending trip iT_{ki}^c can be calculated by Equations (3) and (4):

$$T_{ki}^c = \min \left(\hat{T}_{ki}^v, \hat{T}_{ki}^u \right) \times \gamma_{kij} \quad (3)$$

$$\hat{T}_{ki}^u = \frac{60C \left(\lambda_1 - soc_{ki}^a \right)}{\varsigma_1} \quad (4)$$

where $\hat{T}_{ki}^v$ is the duration of idle time after EB k serves trip i in actual operation, which can be obtained by $\hat{T}_{ki}^v = T_{kj}^D - T_{ki}^a$, min; $\hat{T}_{ki}^u$ is the time required to recharge until battery SOC reaches to λ_1 after EB k ends trip i, min; soc_{ki}^a is the SOC at the end time of trip i, %; C is the battery rated capacity, kWh; ς_1 is the charging rate, kW. It is noticed that $\hat{T}_{ki}^v$ is closely related to T_{ki}^a and has G_i potential values based on Equation (1). Accordingly, $\hat{T}_{ki}^v$ and T_{ki}^c also have G_i potential values separately. The probability that T_{ki}^c takes the g_i-th potential value is denoted by $p(T_{ki}^c = T_{ki}^{c,g_i})$, $1 \leq g_i \leq G_i$.

There is a linear relationship between the increased electricity quantity and the charging time, which can be presented as

$$w_i^+ = \varsigma_1 \times \frac{T_{ki}^c}{60} \quad (5)$$

where w_i^+ is the increased electricity quantity due to recharging in the idle time after trip i, kWh.

2.3 | Stochastic volatility in energy consumption

The energy consumption of an EB during all-day operation time is nonlinear. Specifically, the energy consumption rate per mileage increases gradually with the decrease of battery SOC. There are several factors affecting energy consumptions during the discharging process. We identified three independent variables that have the strongest correlations with energy consumption based on the collected data, including battery SOC at the departure time, trip travel time, and average temperature. Hence, the estimation model for the energy consumption of EB k on the trip i is formulated as follows:

$$\hat{w}_i^- = \hat{\beta}_1 soc_{ki}^d + \hat{\beta}_2 t_i + \hat{\beta}_3 \bar{T}_i^0 + \hat{\beta}_0 \quad (6)$$

where $\hat{w}_i^-$ is the estimated value of the energy consumption of trip i, kWh; soc_{ki}^d is the SOC at the departure time of trip i, %; $\bar{T}_i^0$ is the average temperature during the trip i, °F; $\hat{\beta}_1, \hat{\beta}_2, \hat{\beta}_3$ and $\hat{\beta}_0$ are regression parameters.

The collection of survey data for Equation (6) is described in Section 3.1. Due to the page limit, the detailed regression process of Equation (6) is not included here and will be demonstrated in other papers. Equation (6) gives the structure of the estimation model for trip energy consumption. The values of the parameters would vary with the change of the bus route. In addition, the real data of different trips reveals that even with an identical value of battery SOC at the departure time, trip travel time, and average temperature, there are still differences in energy consumptions. The reason is that the energy consumptions of EBs are also affected by various microscopic factors such as accelerating and decelerating behaviors, intersection queues, dwell times, which are difficult to be directly included in Equation (6). Instead, we use the residual term $\hat{\varepsilon}_i$ to demonstrate the impacts of those factors on the actual energy consumption w_i^- of trip i:

$$w_i^- = \hat{w}_i^- + \hat{\varepsilon}_i \quad (7)$$

The PDF of w_i^- is determined by the features of $\hat{\varepsilon}_i$. The method to determine it can be found in Appendix A.

2.4 | Model development

The objectives of the proposed optimization model include: Minimizing the expectation of delays in trip departure times, the summation of energy consumption expectations, and bus procurement costs. The calculations for the objectives are developed first in this section, and then the optimization model is provided.

2.4.1 | Expectation of delays in trip departure times

The stochastic volatilities in trip travel times have significant impacts on the delays in trip departure times of the continuous trips of EBs. The delay would propagate through the continuous trips served by EB k, until it goes into the idle state or ends the all-day operation. It is assumed that EB k needs to run L continuous trips before going into the idle state. The stochastic volatilities in travel times of the previous (L-1) trips will be accumulated and then pay impacts on the departure time of the L-th trip. Specifically, the number of possible values that could be taken by the departure time of the L-th trip is the summation of numbers of possible values taken by the departure times of the previous (L-1) trips.

The operational state of the trip i run by EB k will affect that of the next trip j. Let T_{kj}^d be the actual departure time of trip j run by EB k. When $\gamma_{kij} = 1$, EB k is arranged to get recharged after ending trip i, and trip j will be served on time, $T_{kj}^d = T_{kj}^D$. When $\gamma_{kij} = 0$, EB k will continuously run trips i and j. If $T_{ki}^a \leq T_{kj}^D$, then $T_{kj}^d = T_{kj}^D$. If $T_{ki}^a > T_{kj}^D$, then there is a delay at the departure time of trip j. To make it clear to describe, let $\hat{T}_{kj}^d$ denote the delayed departure time of EB k on trip j ($\hat{T}_{kj}^d > T_{kj}^D$). The probability that $\hat{T}_{kj}^d$ is the g_i-th possible departure time $\hat{T}_{kj}^{d,g_i}$ is

$$p\left(\hat{T}_{kj}^d = \hat{T}_{kj}^{d,g_i}\right) = p\left(T_{ki}^a = T_{ki}^{a,g_i}\right), \quad \tau_1 < g_i \leq G_i \quad (8)$$

Due to $T_{ki}^{a,\tau_1} = T_{kj}^D$, $T_{ki}^a = T_{ki}^{a,g_i} > T_{kj}^D$ can be satisfied only when g_i is larger than τ_1. If EB k arrives late at the terminal station of trip i ($T_{ki}^a > T_{kj}^D$), it will serve trip j immediately after ending the service on trip i. In such a condition, the number of possible departure times equals the number of possible arrival times, and the probability that $\hat{T}_{kj}^d$ is the g_i-th possible departure time equals the probability that T_{ki}^a is the g_i-th possible arrival time.

If EB k needs to serve the inbound trip l continuously after ending trip j, the delayed departure time on trip l ($\hat{T}_{kl}^d$) will get jointly affected by the travel times of trips i and j. The probability that $\hat{T}_{kl}^d$ is the h-th possible departure time $\hat{T}_{kl}^{d,h}$ is as follows:

$$p\left(\hat{T}_{kl}^d = \hat{T}_{kl}^{d,h}\right) = p\left(\hat{T}_{kj}^a = \hat{T}_{kj}^{a,h}\right) = p\left(T_{ki}^a = T_{ki}^{a,g_i}\right) \times p\left(t_j = t_j^{g_j} \middle| \gamma_{kij} = 0\right), \quad h \geq \tau_2 \quad (9)$$

$$p \left\{ \gamma_{kij} = 0 \right\} = p \left\{ T^a_{ki} > T^D_{kj} - \eta \right\} = \sum_{\tau_3}^{G_i} p \left(T^a_{ki} = T^{a,g_i}_{ki} \right)$$

(10)

where $\hat{T}^a_{kj}$ is the delayed end time of EB k on trip j, and $\hat{T}^a_{kj} > T^D_{kl}$. τ_2 is the possible serial number that T^a_{kj} might take when $T^a_{kj} = T^D_{kl}$. τ_3 is the possible serial number that T^a_{ki} might take when $T^a_{ki} = T^D_{kj} - \eta$.

The expectation of delay in departure time of EB k on any outbound trip j, namely, $E(DD_{kij})$, can be calculated by Equation (11):

$$E \left(DD_{kij} \right) = \sum_{\tau_1} \left(T^a_{ki} - T^D_{kj} \right) p \left(\hat{T}^d_{kj} = \hat{T}^{d,h}_{kj} \right)$$

(11)

where $p(\hat{T}^d_{kj} = \hat{T}^{d,h}_{kj})$ can be calculated by referring to Equation (9). Similarly, the expectation of delay in departure time of EB k on any inbound trip i, $E(DD'_{kji})$, can also be calculated.

2.4.2 | Expectation of trip energy consumptions

The stochastic volatility in the travel time of trip i will directly affect the energy consumption of EB k on the route as well as the duration of idle time and recharging time after ending trip i, accordingly influencing battery SOC at the departure time of trip j, which result in the volatilities in energy consumptions of EB k. If the stochastic volatilities of energy consumptions are not considered, the remaining energy of EB k at the departure time would be overestimated, resulting in the service interruption.

It is assumed that the battery SOC of all EBs at the initial time of daily operation is λ_1. Due to the stochastic volatility in trip travel time, the battery SOCs of EB k on trips i and j are stochastic as well, which are calculated by Equations (12) and (13):

$$soc^a_{ki} = soc^d_{ki} - \frac{w^-_{ki}}{C}, \quad soc^a_{ki} \in \left[soc^{a,\min}_{ki}, soc^{a,\max}_{ki} \right]$$

(12)

$$soc^d_{kj} = soc^a_{ki} + \frac{w^+_{ki}}{C}, \quad soc^d_{kj} \in \left[soc^{d,\min}_{kj}, soc^{d,\max}_{kj} \right]$$

(13)

where soc^a_{ki} and soc^d_{kj} are battery SOCs of EB k at the end time of trip i and the departure time of trip j, %; $soc^{a,\min}_{ki}$, $soc^{a,\max}_{ki}$, $soc^{d,\min}_{kj}$ and $soc^{d,\max}_{kj}$ are the minimum and maximum possible battery SOCs of EB k at the end time of trip i and the departure time of trip j, %, respectively.

Obviously, with a given soc^d_{ki}, the longer travel time of EB k serving trip i would result in a smaller soc^a_{ki}. When $t_i = t^{\max}_i$, $soc^a_{ki} = soc^{a,\min}_{ki}$; when $t_i = t^{\min}_i$, $soc^a_{ki} = soc^{a,\max}_{ki}$. Besides, when $\gamma_{kij} = 1$ and $\hat{T}^v_{ki} \geq \hat{T}^u_{ki}$, we can achieve $soc^{d,\min}_{kj} = soc^{d,\max}_{kj} = \lambda_1$.

As demonstrated in Equation (6), the energy consumption of one trip is affected by its travel time, battery SOC at departure time, and temperature. Let trip j be an example. When t_j takes $t^{g_j}_j$ and soc^d_{kj} takes the g_i-th possible value soc^{d,g_i}_{kj}, the PDF of energy consumption is denoted by $f(w^-_j | t_j = t^{g_j}_j, soc^d_{kj} = soc^{d,g_i}_{kj})$. When $\gamma_{kij} = 0$, the probability of battery SOC at the departure time of trip j taking any possible value is only related to t_i; when $\gamma_{kij} = 1$, the SOC is collectively determined by t_i and T^c_{ki}. Therefore, the probability of battery SOC at the g_i-th departure time $p(soc^d_{kj} = soc^{d,g_i}_{kj})$ and the expectation of energy consumption of EB k on trip $jE(w^-_{kj})$ can be calculated by Equations (14) and (15):

$$p \left(soc^d_{kj} = soc^{d,g_i}_{kj} \right) = p \left(t_i = t^{g_i}_i \right)$$
$$\times \left[p \left(T^c_{ki} = T^{c,g_i}_{ki} \right) p \left(\gamma_{kij} = 1 \right) + p \left(\gamma_{kij} = 0 \right) \right]$$

(14)

$$E \left(w^-_{kj} \right) = \sum_{g_j=1}^{G_j} \sum_{g_i=1}^{G_i} \left[P \left(t_j = t^{g_j}_j \right) p \left(soc^d_{kj} = soc^{d,g_i}_{kj} \right) \right.$$
$$\left. \times \int_W w^-_{kj} f \left(w^-_{kj} \middle| t_j = t^{g_j}_j, soc^d_{kj} = soc^{d,g_i}_{kj} \right) dw^-_{kj} \right]$$

(15)

where W is the fluctuation interval of energy consumption of EB k of trip j. The lower limit of this interval is the energy consumption under $soc^{d,\max}_{kj}$ and $t^{\min}_j$, and the upper limit is the energy consumption under $soc^{d,\min}_{kj}$ and $t^{\max}_j$. Similarly, the expectation of energy consumption of EB k on the trip $iE(w^-_{ki})$ can be calculated.

2.4.3 | Multi-objective optimization model

Besides the traditional bus scheduling constraints, the VSP of EBs includes the constraints of battery remaining energy and charging times. For instance, battery SOC should be maintained within the regulated interval and the bus remaining energy at the departure time of each trip should be sufficient to complete the trip.

The objective function and constraints of the scheduling optimization model are combined and listed as follows:

$$\min Z_1 = \sum_{k=1}^{K} \sum_{i=1}^{N^1} \sum_{j=1}^{N^2} \left[E \left(DD_{kij} \right) \times x_{kij} + E \left(DD'_{kji} \right) \times x'_{kji} \right]$$

(16)

$$\min Z_2 = \sum_{k=1}^{K} \sum_{i=1}^{N^1} \sum_{j=1}^{N^2} \left[E\left(w_{ki}^-\right) + E\left(w_{kj}^-\right) \right] x_{kij} \quad (17)$$

$$\min Z_3 = C_0 \hat{K} \quad (18)$$

$$\hat{K} = \sum_{k=1}^{K} Y_k \quad (19)$$

$$Y_k = 1 - \max\left\{ 1 - \sum_{i=1}^{N^1} \sum_{j=1}^{N^2} x_{kij}, 0 \right\} \quad (20)$$

$$\sum_{k=1}^{K} \sum_{i=0}^{N^1} x_{kij} - 1 = 0 \quad (21)$$

$$\sum_{k=1}^{K} \sum_{j=0}^{N^2} x_{kij} - 1 = 0 \quad (22)$$

$$\varpi - P_k (i \Theta j) \leq 0 \quad (23)$$

$$\varpi - P_k (j \Theta i) \leq 0 \quad (24)$$

$$\delta_1 \frac{N^1 + N^2}{\hat{K}} \leq \sum_{i=1}^{N^1} \sum_{j=1}^{N^2} x_{kij} \leq \delta_2 \frac{N^1 + N^2}{\hat{K}}, \quad \text{when } Y_k = 1 \quad (25)$$

$$\lambda_2 - soc_{ki}^{a,\min} \leq 0 \quad (26)$$

$$\lambda_2 - soc_{kj}^{a,\min} \leq 0 \quad (27)$$

$$x_{kij}, x'_{kji} \in \{0,1\}, \quad i = 1, 2, \dots, N^1;$$
$$j = 1, 2, \dots, N^2; k = 1, 2, \dots, K \quad (28)$$

Equations (16) to (18) demonstrate the objective functions of this optimization model. Equations (16) and (17) are to minimize the expectation of delays in departure times of all trips and the total energy consumption in daily operation, where the calculation method of $E(DD_{kij})$, $E(DD'_{kji})$, $E(w_{ki}^-)$, and $E(w_{kj}^-)$ can be found in Sections 2.2.1 and 2.2.2. Equation (18) is to minimize the bus procurement costs. C_0 is the unit price for EB, RMB/vehicle, and $\hat{K}$ is the number of EBs the route needed, which can be achieved from Equation (19). Note that not all of the K EBs will be deployed in operation. According to Equation (20), $Y_k \in \{0,1\}$, if EB k serves at least one trip, then $Y_k = 1$; otherwise, $Y_k = 0$. Constraints (21) and (22) ensure that one trip can be served once by one bus. Constraints (23) and (24) demonstrate that the time feasibility probability that trips i and j can be served continuously by the same bus should be larger than the acceptable value ϖ, where ϖ is a constant, $0 < \varpi \leq 1$. Constraint (25) is to avoid large differences in the use intensity of EBs in deployment. Notably, the number of trips served by one bus per day should be greater than or equal to δ_1 times of the average trip numbers of each bus and less than or equal to δ_2 times of the average, where $\delta_1 \leq 1.0$ and $\delta_2 \geq 1.0$. Constraints (26) and (27) reveal that battery SOC at the end time of each trip should be greater than the lower safety threshold λ_2. Constraint (28) lists the value ranges of some parameters.

2.5 | Solution algorithm

There are three optimization objectives in the model. Let us take Z_2 as an example. Trip energy consumption is affected by multiple factors, such as the initial SOC at the departure time and the trip travel time. The initial SOC is determined by the energy consumption of the last trip, the charging strategy, and the stochastic trip travel time. Obviously, the calculation equation for Z_2 is a nonlinear function. It is hard to directly solve the nonlinear optimization model with multiple independent variables.

In addition, three objectives in the model restrict each other. Specifically, to obtain better on-time performance and less energy consumption, it is required to select a larger time feasibility probability for continuous trips and arrange longer charging time, which leads to the increase in EB fleet size and procurement costs. Hence, no solution may make all three objectives optimal simultaneously. However, there exists a set of Pareto optimal solutions.

The nondominated sorting genetic algorithm with the elitist strategy (NSGA-II) shows strong global search ability and robustness (Deb et al., 2002; Yang et al., 2007; Zeng et al., 2019). This algorithm applies the crowded degree calculation and a rapid nondominated sorting

procedure to reduce the computational complexity while maintaining the population diversity. Besides, the algorithm adds the competition between parent and child populations during the selection procedure to improve the probability of maintaining elite individuals.

The steps are listed as follows of how to implement NSGA-II to solve the proposed optimization model:

Step 1: Let $b = 0$ and the integer coding mechanism is adopted to encode bus scheduling plans. The chromosome length equals the number of total trips in operation, which is denoted by $N^1 + N^2$. The former N^1 is the number of inbound trips and the latter N^2 is the number of outbound trips. The value of each code is the serial number of buses serving this trip, which belongs to $[1, K]$. Different codes taking the same value refers that those trips are served by the same EB. For example, the chromosome [1 3 4 2 1 | 2 1 3 4 3] represents five inbound and five outbound trips in one day. From the codes, we can obtain the following information: EB1 is deployed to serve the first and fifth inbound trips and the second outbound trip; EB 2 is deployed to serve the fourth inbound trip and the first outbound trip, and so forth.

Step 2: Population initialization. Fifty bus scheduling plans that satisfy Constraints (21) to (28) are stochastically selected to form the initial population (the first parent generation).

Step 3: The crossover probability is set to be 0.7 and the mutation probability to be 0.01. Roulette wheel selection, uniform crossover, and uniform mutation are utilized for the genetic procedure. The mutated population is recorded as a child population. The population Ψ_b is achieved by combining the parent and child populations.

Step 4: The constraint violation value $CV(X)$ is used to calculate the degree of plan X that violates the constraints.

$$CV(X) = \sum_{v=1}^{6} \langle \varphi_v(X) \rangle + \sum_{u=1}^{2} |\phi_u(X)| \quad (29)$$

where $\varphi_v(X)$ is the nonequality constraint in the standardization model; $\phi_u(X)$ is the equality constraint in the model (e.g., Constraints (21) and (22)). v and u are the serial numbers for nonequality and equality constraints. In this study, $1 \le v \le 6$, $1 \le u \le 2$. If $\varphi_v(X) \le 0$, then $\langle \varphi_v(X) \rangle = 0$; otherwise, $\langle \varphi_v(X) \rangle = |\varphi_v(X)|$. For a feasible scheduling plan X, $CV(X) = 0$. For a nonfeasible scheduling plan, the smaller the $CV(X)$, the better the plan. Judge whether plan X is feasible according to Equation (29). If yes, go to step 5; otherwise, go to step 9.

Step 5: Nondominated sorting procedure is used to calculate the nondominant level of bus scheduling plan R. For example, when three objectives (shown in Equations 16–18) of plan 1 from the population precede all objectives of plan 2, it is thought that plan 1 dominates plan 2. The number of plans that dominate plan R is denoted by n_R. The plans with $n_R = 0$ are put in a list H_i, which is called the first nondominated level.

Step 6: A set of plans in H_i that are dominated by the plan h is s_h, and all plans in s_h are checked. For each plan y in s_h, we calculate n_y and do $n_y = n_y - 1$; then, any plan y with $n_y = 0$ will be put into the list H_{i+1}.

Step 7: $i = i+1$; go back to step 6 until each bus scheduling plan R is assigned to a nondominated level.

Step 8: Crowded degree calculation. The crowded degrees of individuals in the same nondominated level are initialized to be 0, which means that $L_d[r] = 0$. $L_d[r]$ is the crowded degree of an individual r. Then, crowded degrees of all marginal individuals are set as a very high value. For a nonmarginal individual, its crowded degree $L_d[r]$ is updated by Equation (30):

$$L_d[r] = \frac{L(r+1, z) - L(r-1, z)}{f_z^{\max} - f_z^{\min}} \quad (30)$$

where $L(r, z)$ is the z-th objective value of the rth individual. $f_z^{\max}$ and $f_z^{\min}$ are the maximum and minimum of the z-th objective value. Then, the values of individuals of the z-th ($z = 1, 2, 3$) objective are separately sorted in the ascending order. The objectives are listed in Equations (16) to (18).

Step 9: Comparison among individuals. For plans 1 and 2, if the level of plan 1 is lower than or equal to that of plan 2 (level 1 is the best level), and the crowded degree of plan 1 is larger than or equal to that of plan 2, then it is said to plan 2 is Pareto dominated by plan 1.

Plan 2 is constrained-dominated by plan 1 when any of the following conditions is satisfied: (i) Both plans 1 and 2 are feasible solutions, and plan 2 is Pareto-dominated by plan 1. (ii) Plan 1 is a feasible solution, while plan 2 is not. (iii) Neither plan 1 nor plan 2 is a feasible solution, but CV(1) < CV(2). The first 20 plans ranked from top to bottom are selected to form a parent population of the next generation.

Step 10: Let $b = b + 1$ and go back to step 3. Stop the iteration when the objective values of the parent

and child population are entirely identical, and these values remain unchanged for at least 5 times.

After obtaining a set of Pareto optimal solutions, operators will consider these three objective functions in order of priority to select an optimal solution in actual bus operation. Typically, reasonable vehicle scheduling plans with fewer EBs needed are considered first for the bus procurement costs. Then, the plans with the least expectation of delays in departure times are selected considering the service quality of the bus line. Finally, an optimal solution is adopted to minimize the summation of energy consumption expectations and determine the idle times and charging plan.

The computational burden of the solution algorithm will become larger with the increase in fleet size and the number of total trips. However, the main purpose of this study is to generate the optimal static scheduling plan for EBs on a fixed route. For this research scenario, even several-minute computational time is acceptable. Hence, the threshold for the computational time does not need to be set as a small value for our algorithm. In another word, the proposed algorithm is capable of satisfying the requirements on the computational burden and suitable for the scheduling problem of a bus route with a large fleet size and high dispatching frequency. In addition, with the increase of fleet size and the total number of trips, the chromosome length will also increase significantly, which could easily generate local optimal solutions, leading to the deterioration of solution quality. In such a condition, it is better to increase the population size to improve the solution quality.

3 | NUMERICAL EXAMPLE

3.1 | Data input

We conducted numerical tests to verify the performance of the proposed optimization method based on the EB route 108 in Meihekou City, Jilin Province, China. The travel length of route 108 is 7.9 km per direction, consisting of 24 stations as demonstrated in Figure 2. EBs running on this route were bought in June 2018 and equipped with $LiFePO_4$ batteries. The weight, size, and capacity are 82,000 kg, 8500 × 2500 × 3215 mm^3, and 60 passengers, respectively. These buses run between two terminals: Leibang residence and the building material market. Both terminals have sufficient land resources to install charging devices for EBs. The direction from the building material market to Leibang residence is denoted as the inbound direction and the opposite as the outbound direction. We collected operating data from 1520 trips on route 108 in
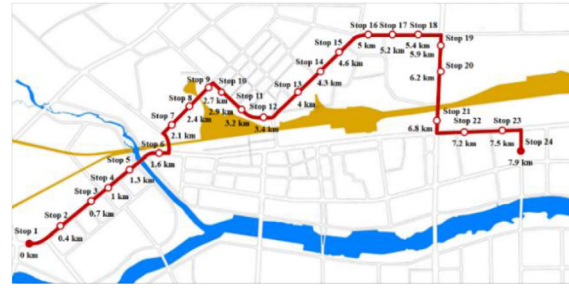

FIGURE 2 Sketch diagram of route 108 in Meihekou City, China

15 workdays during January 2020, including trip travel time, energy consumption, departure time, end time, average temperature and battery state of health (SOC), and so forth. According to the survey data, the state of health (SOH) of the EB is about 0.975. The minimum and maximum temperatures are 19 and 30.2° F, respectively. Passenger demands in peak hour in the inbound and outbound direction are 1350 and 1140 passengers/h, respectively.

The daily operation time is divided into seven periods for this route. The departure time of the first trip is 5:30 a.m. and that of the last one is 11:55 PM. The scheduled departure timetable of route 108 is listed in Appendix B. There are 110 inbound trips and 110 outbound trips, namely, $N^1=N^2=110$. The dispatching headways are shown in Table 1 as well as the number of trips in each period. The average values, standard deviations, and 80th percentiles of trip travel time of inbound and outbound trips in each period are demonstrated in Tables 2 and 3.

The statistical parameters in Tables 2 and 3 are achieved from real data analysis, and here we take the time period "5:30–7:00 a.m." in Table 2 as an example to illustrate the process of obtaining those parameters as well as their meanings. The travel time of inbound trip i is denoted by t_i, which is a discrete variable of which the value fluctuates within a certain interval with a 1-min step. Based on our investigation data, the minimum and maximum travel times during 5:30–7:00 a.m. are 21 and 33 min respectively. Thus, we can get $t_i \in [21, 22, 23, ..., 31, 32, 33]$ for the time period "5:30–7:00 a.m.," which is recorded as $t_i \in [21, 33]$ in Table 2. G_i denotes the number of possible values for t_i, and here, G_i equals 13. During this time period, the average value and standard deviation of t_i are 28 and 2 min, respectively, obtained from real data analysis. The 80th percentile of t_i is 29 min.

In our research, to alleviate battery depreciation, EBs make use of idle time to get recharged with slow charging mode. The charge rate is 0.2 C, which means that it takes 5 hr to charge a battery from SOC = 0 to its rated capacity. Thus, $\varsigma_1 = 32.4$ kW.

TABLE 1 Dispatching headway and number of trips in each time period

q	Starting time	Ending time	Headway (min)	Number of trips
1	5:30 a.m.	7:00 a.m.	15	14
2	7:00 a.m.	9:00 a.m.	5	48
3	9:00 a.m.	11:30 a.m.	12	24
4	11:30 a.m.	1:30 p.m.	8	30
5	1:30 p.m.	4:30 p.m.	14	34
6	4:30 p.m.	7:00 p.m.	6	46
7	7:00 p.m.	9:55 p.m.	15	24

TABLE 2 Statistical parameters of inbound bus trip travel time on route 108

q	Time period	G_i	t_i	Average (min)	Standard deviation (min)	80th percentile (min)
1	5:30–7:00 a.m.	13	[21,33]	28	2	29
2	7:00–9:00 a.m.	16	[26,41]	35	3	38
3	9:00–11:30 a.m.	14	[22,35]	31	3	33
4	11:30 a.m.–1:30 p.m.	15	[24,38]	32	3	34
5	1:30–4:30 p.m.	14	[22,35]	29	3	32
6	4:30–7:00 p.m.	16	[26,41]	34	3	36
7	7:00–9:55 p.m.	16	[21,36]	29	3	32

Based on the method in step 3 of Appendix A, we found that 61.696 > 16.919 ($\Lambda R^2 > \chi_\alpha^2(9)$) and heteroscedasticity exists. Thus, the weighted least square method is adopted to obtain the fitted energy consumption estimation model as follows:

$$\hat{w}_i^- = -3soc_i^d + 0.270t_i - 0.085\bar{T}_i^0 + 0.853, \ \ R^2 = 0.99 \tag{31}$$

The variance around this regression line is 1.87 and the student's t-test statistics of parameters at 0.05 confidence level are 19.222, 33.903, and –14.921, respectively. Hence, they all have significant impacts on trip energy consumption.

The average temperature of each hour during operation time is listed in Table 4. The values of other parameters in the model are in Table 5. Actual trip energy consumption is

TABLE 3 Statistical parameters of outbound bus trip travel time on route 108

q	Time period	G_j	t_j	Average (min)	Standard deviation (min)	80th percentile (min)
1	5:30–7:00 a.m.	12	[21,32]	27	2	28
2	7:00–9:00 a.m.	17	[25,41]	34	3	36
3	9:00–11:30 a.m.	14	[22,35]	29	3	32
4	11:30 a.m.–1:30 p.m.	16	[24,39]	33	3	35
5	1:30–4:30 p.m.	15	[23,37]	30	2	32
6	4:30–7:00 p.m.	17	[26,42]	36	3	38
7	7:00–9:55 p.m.	16	[22,37]	30	3	33

TABLE 4 The average temperature of each hour during the operating period

Starting time	5:00 a.m.	6:00 a.m.	7:00 a.m.	8:00 a.m.	9:00 a.m.	10:00 a.m.	11:00 a.m.	12:00 p.m.	13:00 p.m.
$\bar{T}^0$ (°F)	21.34	21.79	22.16	22.18	22.40	22.40	22.21	21.93	21.79
Starting time	2:00 p.m.	3:00 p.m.	4:00 p.m.	5:00 p.m.	6:00 p.m.	7:00 p.m.	8:00 p.m.	9:00 p.m.	10:00 p.m.
$\bar{T}^0$ (°F)	21.48	21.20	20.84	20.68	20.36	20.04	19.98	19.66	19.58

TABLE 5 Values of some important input parameters of the model

Parameters	Descriptions	Values
K	Maximum number of equipped electric buses (EBs)	19
$[\lambda_2, \lambda_1]$	Battery state of charge (SOC) interval	[20%, 80%]
C	Rated capacity of the battery	162 kWh
η	—	15 min
δ_1/δ_2	—	0.90/1.10
C_0	Purchase cost	650,000 RMB

not the input parameter of the optimization model. Thus, the values in different time periods are not given. According to survey data, in off-peak hours, the maximum and minimum trip energy consumptions are 7.3 and 3.4 kWh, respectively. The average and standard deviations are 4.23 and 1.14 kWh.

3.2 | Optimal plan

NSGA-II is implemented to solve the proposed vehicle scheduling model with $\varpi=0.80$. Experimental tests are performed in a general-purpose computer with Intel Core i5-9400F CPU @2.90 GHz and 8GB RAM. The optimal solution is achieved within 130 iterations and the computational time is 41.73 s. For the optimal plan, $Z_1 = 0.63$ min, $Z_2 = 1229.8$ kWh, $Z_3 = 10,400,000$ RMB. Based on the solution, 16 EBs should be deployed into daily operations, namely, $\hat{K} = 16$.

Except for the above optimal solution, the other Pareto optimal solution (denoted as the suboptimal solution) is adopted here to conduct the comparison. The suboptimal solution needs 17 EBs, and $Z_1 = 0$ min, $Z_2 = 1205.2$ kWh, $Z_3 = 11,050,000$ RMB. Comparing these two solutions, it can be found that the optimal solution can save the procurement cost of one bus, which is 650,000 RMB. Compared with the suboptimal solution, the growths of expectation of delays in departure times and summation of energy consumption expectations under the optimal solution are 0.63 min and 24.6 kWh, respectively. The growths are significantly smaller than the bus purchase cost C_0. Therefore, we choose the optimal solution as the vehicle scheduling scheme of line 108 rather than the suboptimal solution.

The trip set for each odd-numbered bus is demonstrated in Table 6. To ensure the normal turnover of the line, it is usually necessary for two EBs to depart from both terminals at the same time, serving the inbound and outbound trips, respectively, so that each even-numbered bus, in turn, serves the same trip number as the last bus (odd-numbered) but in the opposite direction. The departure time of each trip can be achieved in Appendix B. From Table 6 we can conclude that 12 buses need to run 14 trips per day and four buses need to run 13 trips per day. Let us take EB1 as an instance. It is allocated to serve the following trips in sequence: The first inbound trip at 5:30 a.m., the ninth outbound trip at 7:10 a.m., the 17th inbound trip at 7:50 a.m., the 25th outbound trip at 8:30 a.m., and so forth. Combining the fluctuation of trip times in each period, we can also achieve the maximum expectation of total travel times for each bus among the bus fleet as 451 min ($k = 7$, 9, 11) and the minimum as 414 min ($k = 14$), which illustrates that the differences in use intensity among buses are minor.

As described in Section 2.1, the stochastic volatilities have significant impacts on the vehicle scheduling of EBs. Let us take EB1 as an example again. Table 7 displays the charging plan of EB1, including idle times, charging times, and fluctuation intervals of battery SOC before and after charging, considering the stochastic volatilities in trip travel times and energy consumptions. The starting charging time is determined by the actual end time of a trip.

EB1 is required to serve multiple continuous trips and cannot get recharged after ending any trip during peak hours (7:00–9:00 a.m., 4:30–7:00 p.m.); thus, the battery SOC at the departure time of the next trip is stochastic. During nonpeak hours, EB1 has long idle times for recharg-

TABLE 6 Trip numbers allocated to each EB

EB No.	Trip numbers
1	$1^+ \to 9^- \to 17^+ \to 25^- \to 33^+ \to 41^- \to 49^+ \to 57^- \to 65^+ \to 73^- \to 81^+ \to 89^- \to 97^+ \to 105^-$
3	$2^+ \to 10^- \to 18^+ \to 26^- \to 34^+ \to 42^- \to 50^+ \to 58^- \to 66^+ \to 74^- \to 82^+ \to 90^- \to 98^+ \to 106^-$
5	$3^+ \to 11^- \to 19^+ \to 27^- \to 35^+ \to 43^- \to 51^+ \to 59^- \to 67^+ \to 75^- \to 83^+ \to 91^- \to 99^+ \to 107^-$
7	$4^+ \to 12^- \to 20^+ \to 28^- \to 36^+ \to 44^- \to 52^+ \to 60^- \to 68^+ \to 76^- \to 84^+ \to 92^- \to 100^+ \to 108^-$
9	$5^+ \to 13^- \to 21^+ \to 29^- \to 37^+ \to 45^- \to 53^+ \to 61^- \to 69^+ \to 77^- \to 85^+ \to 93^- \to 101^+ \to 109^-$
11	$6^+ \to 14^- \to 22^+ \to 30^- \to 38^+ \to 46^- \to 54^+ \to 62^- \to 70^+ \to 78^- \to 86^+ \to 94^- \to 102^+ \to 110^-$
13	$7^+ \to 15^- \to 23^+ \to 31^- \to 39^+ \to 47^- \to 55^+ \to 63^- \to 71^+ \to 79^- \to 87^+ \to 95^- \to 103^+$
15	$8^+ \to 16^- \to 24^+ \to 32^- \to 40^+ \to 48^- \to 56^+ \to 64^- \to 72^+ \to 80^- \to 88^+ \to 96^- \to 104^+$

Note: "+" denotes the inbound trip, and "−" denotes the outbound trip.

TABLE 7 Charging plan of EB1 under the impact of travel time and energy consumption stochastic volatilities

Departure time	Idle time (min)	Charging time (min)	Battery SOC at the trip ending time (%)	Battery SOC after charging (%)
5:30 a.m.	[67,79]	[4,10]	[76.6,78.6]	80.0
7:10 a.m.	[−1,15]	0	[75.3,78.0]	[75.3,78.0]
7:50 a.m.	[−1,14]	0	[70.5,75.7]	[70.5,75.7]
8:30 a.m.	[13,29]	0	[65.6,73.6]	[65.6,73.6]
9:24 a.m.	[61,74]	[24,55]	[61.6,71.9]	80.0
11:00 a.m.	[37,50]	[5,11]	[76.3,78.5]	80.0
12:12 p.m.	[26,40]	[6,13]	[75.8,78.1]	80.0
1:16 p.m.	[49,64]	[6,13]	[75.6,78.1]	80.0
2:44 p.m.	[53,66]	[5,11]	[76.2,78.4]	80.0
4:12 p.m.	[24,38]	[5,12]	[75.9,78.2]	80.0
5:13 p.m.	[7,22]	0	[75.2,77.7]	[75.2,77.7]
6:01 p.m.	[6,22]	0	[70.1,75.4]	[70.1,75.4]
6:49 p.m.	[70,85]	[21,45]	[65.1,73.0]	80.0
8:40 p.m.	–	[5,12]	[75.8,78.3]	80.0

Note: The negative idle time indicates the possible delay in departure time of EB1 on the next trip; the charging time that equals 0 denotes that there is no charging arranged during this idle time.

ing. Specifically, after the end of the inbound trips departing at 9:24 a.m. and 6:49 p.m., the required maximum recharging times are, respectively, 55 and 45 min while the assigned minimum idle times are 61 and 70 min based on the optimal scheduling plan. This ensures that the battery SOC recovers to 80% after recharging, reaching the goal of saving energy. Even with a low charging rate (0.2 C) applied in this paper, the recharging times during nonpeak hours are no longer than 15 min, indicating that such a charging plan effectively avoids the battery life depreciation problem caused by high charging rate.

During the vehicle scheduling process, continuous trips served by the same EB should meet the time feasibility constraints as shown in Equations (23) and (24). These requirements of time feasibility are affected by the selection of ϖ, which consequently has a significant impact on the number of EBs deployed in operation and the on-time performance of this route. In this paper, the travel time

of each trip is a discrete variable fluctuating within a certain interval with a 1-min step. The continuous trips i and j served by EB k are used as an example here to explain the impact of various values of ϖ. t_i is assumed to vary within [20 min, 30 min]. When t_i is 26 min, $P_k(i \Theta j) = 0.80$, and when t_i increases to 27 min, $P_k(i \Theta j) = 0.86$. Thus, when ϖ is 0.81 and 0.86, t_i remains 27 min, and accordingly, no difference exists in the scheduling plans generated with such ϖ. That is when ϖ takes the value from a certain interval, the numbers of buses needed $\hat{K}$, and the expectation of delays in departure times Z_1 of the generated scheduling plans remain unchanged as shown in Table 8.

It is concluded that Z_1 decreases and $\hat{K}$ increases with the growth of ϖ. To be specific, when $\varpi \in (0.99, 1.0]$, all EBs can depart on schedule. Under this circumstance, it is required to allocate 18 EBs into operation. When $\varpi \in (0.97, 0.99]$ and $\varpi \in (0.72, 0.97]$, 17 and 16 EBs should

TABLE 8 Corresponding $\hat{K}$ and Z_1 under different intervals of ϖ

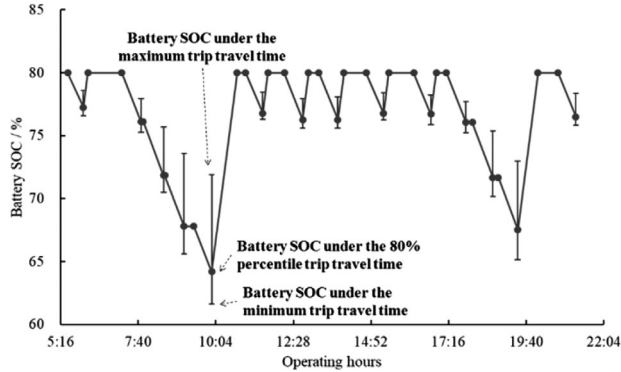| ϖ	$\hat{K}$	Z_1 (min)
[0.50, 0.59]	14	45.74
(0.59, 0.72]	15	14.88
(0.72, 0.97]	16	0.63
(0.97, 0.99]	17	0.25
(0.99, 1.0]	18	0

FIGURE 3 Battery state of charge variation curve of EB1 during all-day operation time

be deployed. The corresponding expectations of delays in departure times are both less than 1 min, which indicates good on-time performance. However, when $\varpi \in$ (0.59, 0.72] and $\varpi \in$ [0.50, 0.59], the demand for EBs is relatively low, but the on-time performance is terrible in these conditions. With the comprehensive consideration of procurement costs and on-time performance, it is logical for ϖ to take the value from (0.72, 0.97] on route 108. Based on the corresponding generated scheduling plan, 16 EBs are required and Z_1 is only 0.63.

3.3 | Results analysis and evaluation

Based on the generated trip set and charging plan in Section 3.2, the variation curve of battery SOC is calculated for EB1 as shown in Figure 3. Travel time is considered to be stochastic for each trip in our study; thus, the SOC at the end time of each trip is also stochastic. In Figure 3, the solid dot marks the SOC value under the 80th percentile value of the travel time variation range of each trip. The top of each vertical line denotes the SOC value under the maximum value of the trip travel time. The bottom is the SOC value under the minimum value of the trip travel time. Thus, each vertical line denotes the fluctuation range of the SOC at the end time of each trip.

From Figure 3 we can find that during peak hours EB1 is required to continuously run three or four trips, the

impact of stochastic volatilities of previous trips will be accumulated, and extend the fluctuation intervals of battery SOC of the following trips. Take the morning peak hours as an instance. EB1 needs to run four continuous trips, of which the SOC fluctuation intervals at end times are [75.3%, 78.0%], [70.5%, 75.7%], [65.6%, 73.6%] and [61.6%, 71.9%], respectively. The fluctuation range increases gradually from 2.7% to 10.3%. However, during nonpeak hours, there is always a long idle time after each trip, and the stochastic volatilities of the previous trip will not propagate to the following one. Thus, the fluctuation range of battery SOC at the end time of each trip is quite small. For the trips of which departure times are 11:00 a.m. and 12:12 p.m., fluctuation intervals of battery SOC at their end times are separately [76.3%, 78.5%] and [75.8%, 78.1%], and fluctuation ranges are 2.2% and 2.3%.

Besides, by combining the probability distributions of all trips, we achieve the fluctuation intervals of mean values of the normal distribution $\hat{w}_i^-$ and their expectations as listed in Table 9. The average value of expectations of all trips during nonpeak hours and peak hours are 4.8 and 5.9 kWh, respectively. Fluctuation intervals are wider and expectations are larger during peak hours than those during other periods.

This proves that reasonable idle times can be generated by optimizing vehicle scheduling plans, and those idle times can "jeopardize" the propagation of stochasticity, reduce energy consumptions and fluctuation ranges of battery SOC, and further improve the robustness of scheduling plans.

In general, the battery SOCs among EBs vary between 60% and 80% during operation time, and the SOCs are always maintained within the preset intervals, which reduces the damage to the battery. Two reasons are concluded for battery SOCs remaining with high values: (i) The length of route 108 is short. The energy consumption of each trip is little. Even EB1 served four continuous trips during peak hours, its battery SOC only dropped from 80% to 61.6%. (ii) One of the optimization objectives in this paper is to minimize the expectation of total energy consumption of all buses during daily operation, and the high SOC level at departure time is helpful to reduce the energy consumption of each trip. As observed from Equation (31),

TABLE 9 Fluctuation intervals of energy consumptions of all trips by EB1 and expectations

i	T_{ki}^{D}	$\hat{w}_i^-$ (kWh)	Expectations (kWh)	j	T_{kj}^{D}	$\hat{w}_j^-$ (kWh)	Expectations (kWh)
1	5:30 a.m.	[2.3, 5.5]	4.1	9	7:10 a.m.	[3.3, 7.6]	5.7
17	7:50 a.m.	[3.7, 7.8]	6.0	25	8:30 a.m.	[3.4, 7.9]	5.9
33	9:24 a.m.	[2.7, 6.4]	5.1	41	11:00 a.m.	[2.5, 6.0]	4.5
49	12:12 p.m.	[3.1, 6.8]	5.1	57	1:16 p.m.	[3.1, 7.1]	5.4
65	2:44 p.m.	[2.6, 6.1]	4.6	73	4:12 p.m.	[2.9, 6.7]	4.7
81	5:13 p.m.	[3.7, 7.8]	5.8	89	6:01 p.m.	[3.8, 8.2]	6.1
97	6:49 p.m.	[3.9, 8.1]	5.7	105	8:40 p.m.	[2.7, 6.7]	5.0

if trip i and trip $i+1$ has the same temperature and travel time, but the SOC at the departure time of trip i is 10% higher than that of trip $i+1$, then the energy consumption of trip i is 0.3 kWh less than that of trip $i+1$.

The battery fading rate and actual service life of an EB are uncertain due to the influence of the initial SOC, DoD, and environmental temperature. Lam and Bauer (2013) tested the effect of the initial SOC and DoD on the battery cycle life at the same temperature, and a practical capacity fading empirical model was proposed as Equation (32).

$$\begin{cases} \xi_k = 365 \sum_{n=1}^{N} \left[w_{kn}^- \cdot \left(\theta_1 SOC_{dev,n}^d \times e^{\theta_2 SOC_{avg,n}^d} + \theta_3 e^{\theta_4 SOC_{dev,n}^d} \right) \right] \\ N = \sum_{i=1}^{N1} \sum_{j=1}^{N2} x_{kij} \end{cases}$$

$$(32)$$

where ξ_k is the total capacity fade of EB k per year, kWh; n is the trip number for EB k, $1 \le n \le N$. w_{kn}^- is the energy consumption of EB k on trip n, kWh; $SOC_{avg,n}^d$ is the average SOC on trip n, and it equals the average of the SOC when EB k departs from the original station and the SOC when EB k arrives at the terminal station. $SOC_{dev,n}^d$ is the deviation from the average SOC of EB k on trip n and it equals the SOC when EB k departs from the original station minus $SOC_{avg,n}^d$. $\theta_1, \theta_2, \theta_3$, and θ_4 equals -4.09×10^{-4}, -2.167, 1.408×10^{-5}, and 6.13, respectively.

Comparisons on the battery cycle life between the proposed scheduling method (method A) and the current scheduling method (method B) of route 108 are conducted.

Method A: The EB scheduling plan is generated by the optimization model, and the EB can be recharged in idle times while the SOC is limited to [20%, 80%].

Method B: The EB scheduling plan is generated by the optimization model. However, the EB would not get recharged in idle times if it has sufficient remaining electricity for the following trips. Otherwise, the EB would be fully charged.

The battery fading rate under method A is 0.438 kWh per year, while that under method B is 1.424 kWh per year, which indicates a 69.2% reduction in the battery fading rate when switching from the current scheduling method to the proposed scheduling method. It should be noted that in

Equation (32), only SOC is considered. In practice, many other factors also play an impact on the battery fading rate.

4 CONCLUSION

In this study, the impacts of stochastic volatilities in travel times and energy consumptions during operation on vehicle scheduling of EBs were taken into consideration. On this basis, we proposed the charging strategy to recharge buses during their idle times, formulated a model describing the stochastic volatilities in energy consumptions, and developed a battery SOC calculation method under the influences of the stochastic volatilities in travel times and energy consumptions. An optimization model was built with the objectives of minimizing the expectation of delays in trip departure times, the summation of energy consumption expectations, and bus procurement costs. We utilized an actual bus route as an example to demonstrate and verify the proposed method. The following conclusions were drawn in this study:

(i) The stochastic volatilities in travel times and energy consumptions during daily operation will propagate through continuous trips served by the same bus. However, reasonable idle times can be generated by optimizing the vehicle scheduling plan, and it is helpful to stop the accumulation of stochastic volatilities, reduce fluctuation ranges of battery SOCs, and improve the robustness of the optimal scheduling plan.

(ii) Collaboratively optimizing vehicle scheduling and charging plan can reduce the EB fleet and delay time while meeting the route operation needs and keeping the battery SOCs at a relatively high level so as to reduce energy consumptions and prolong battery cycle life.

(iii) It is revealed by the proposed energy consumption estimation model that the low SOC at departure times will increase energy consumptions on the route.

Thus, it is not recommended to arrange a bus to serve multiple continuous trips. Instead, idle times should be scheduled wisely for EBs to get recharged, which is helpful to reduce energy consumptions. This is the main reason why there are differences in vehicle scheduling plans for electric and fuel buses.

It is assumed in this study that there are enough charging piles so that buses do not need to wait for charging. However, when the number of charging piles is not sufficient, the waiting time for EBs will be prolonged, which would affect vehicle scheduling and charging plans. In the future, we will consider the impacts of the number and locations of charging piles and conduct modifications on the proposed optimization model. In addition, with the increase of fleet size and number of trips, the NGSA-II algorithm may not obtain a global optimal solution for the optimization model. A more reliable solution algorithm should be studied in the future.

ORCID

Yiming Bie https://orcid.org/0000-0003-4651-1570
Jinhua Ji https://orcid.org/0000-0003-2923-4663
Xiangyu Wang https://orcid.org/0000-0001-8718-6941
Xiaobo Qu https://orcid.org/0000-0003-0973-3756

REFERENCES

Adeli, H., & Jiang, X. (2009). *Intelligent infrastructure–neural networks, wavelets, and chaos theory for intelligent transportation systems and smart structures*, Boca Raton, FL: CRC Press.

Adeli, H., & Ghosh-Dastidar, S. (2004). Mesoscopic-wavelet freeway work zone flow and congestion feature extraction model. *Journal of Transportation Engineering—ASCE*, *130*(1), 94–103.

Adler, J. D. (2014). *Routing and scheduling of electric and alternative-fuel vehicles* (Doctoral dissertation). https://repository.asu.edu/attachments/134788/content/Adler_asu_0010E_13619.pdf.

Al-Ogaili, A. S., Ramasamy, A., Hashim, T. J. T., Al-Masri, A. N., Hoon, Y., Jebur, M. N., Verayiah, R., & Marsadek, M. (2020). Estimation of the energy consumption of battery driven electric buses by integrating digital elevation and longitudinal dynamic models: Malaysia as a case study. *Applied Energy*, *280*, 115873.

Amberg, B., Amberg, B., & Kliewer, N. (2019). Robust efficiency in urban public transportation: Minimizing delay propagation in cost-efficient bus and driver schedules. *Transportation Science*, *53*(1), 89–112.

An, K. (2020). Battery electric bus infrastructure planning under demand uncertainty. *Transportation Research Part C: Emerging Technologies*, *111*, 572–587.

Basma, H., Mansour, C., Haddad, M., Nemer, M., & Stabat, P. (2020). Comprehensive energy modeling methodology for battery electric buses. *Energy*, *207*, 118241.

Bie, Y., Xiong, X., Yan, Y., & Qu, X. (2020). Dynamic headway control for high-frequency bus line based on speed guidance and intersection signal adjustment. *Computer-Aided Civil and Infrastructure Engineering*, *35*(1), 4–25.

Bunte, S., & Kliewer, N. (2009). An overview on vehicle scheduling models. *Public Transport*, *1*(4), 299–317.

Ceder, A. (2002). Urban transit scheduling: Framework, review and examples. *Journal of Urban Planning and Development—ASCE*, *128*(4), 225–244.

Ceder, A. (2011). Public-transport vehicle scheduling with multi vehicle type. *Transportation Research Part C: Emerging Technologies*, *19*(3), 485–497.

Chediak, M. (2018). *EBs will take over half the world fleet by 2025*. https://www.bloomberg.com/news/articles/2018-02-01/electricbuses-will-take-over-half-the-world-by-2025.

Deb, K., Pratap, A., Agarwal, S., & Meyarivan, T. (2002). A fast and elitist multiobjective genetic algorithm: NSGA-II. *IEEE Transactions on Evolutionary Computation*, *6*(2), 182–197.

Dzikiy, P. (2019). *Bogotá, Colombia to add nearly 600 EBs in 2020, makes claim for largest fleet in Latin America*. https://electrek.co/2019/06/11/bogota-colombia-electric-buses.

El-Taweel, N. A., Zidan, A., & Farag, H. E. Z. (2020). Novel electric bus energy consumption model based on probabilistic synthetic speed profile integrated with HVAC. *IEEE Transactions on Intelligent Transportation Systems*. doi: 10.1109/TITS.2020.2971686

Fusco, G., Alessandrini, A., Colombaroni, C., & Valentini, M. P. (2013). A model for transit design with choice of electric charging system. *Procedia-Social and Behavioral Sciences*, *87*, 234–249.

Gao, K., Yang, Y., Li, A., Li, J., & Yu, B. (2021). Quantifying economic benefits from free-floating bike-sharing systems: A trip-level inference approach and city-scale analysis. *Transportation Research Part A: Policy and Practice*, *144*, 89–103.

Gao, K., Yang, Y., Sun, L., & Qu, X. (2020). Revealing psychological inertia in mode shift behavior and its quantitative influences on commuting trips. *Transportation Research Part F: Traffic Psychology and Behaviour*, *71*, 272–287.

Ghosh-Dastidar, S., & Adeli, H. (2006). neural network-wavelet micro-simulation model for delay and queue length estimation at freeway work zones. *Journal of Transportation Engineering—ASCE*, *132*(4), 331–341.

Guo, C., Wang, C., & Zuo, X. (2019). A genetic algorithm based column generation method for multi-depot electric bus vehicle scheduling. *Proceedings of the Genetic and Evolutionary Computation Conference Companion*, Prague, Czech Republic (pp. 367–368).

Hadjar, A., Marcotte, O., & Soumis, F. (2006). A branch-and-cut algorithm for the multiple depot vehicle scheduling problem. *Operations Research*, *54*(1), 130–149.

He, H., Yan, M., Sun, C., Peng, J., Li, M., & Jia, H. (2018). Predictive air-conditioner control for electric buses with passenger amount variation forecast. *Applied Energy*, *227*, 249–261.

He, Y., Song, Z., & Liu, Z. (2019). Fast-charging station deployment for battery electric bus systems considering electricity demand charges. *Sustainable Cities and Society*, *48*, 101530.

Ibarra-Rojas, O. J., Giesen, R., & Rios-Solis, Y. A. (2014). An integrated approach for timetabling and vehicle scheduling problems to analyze the trade-off between level of service and operating costs of transit networks. *Transportation Research Part B: Methodological*, *70*, 35–46.

Jana, A., Shaver, G. M., & García, R. E. (2019). Physical, on the fly, capacity degradation prediction of LiNiMnCoO2-graphite cells. *Journal of Power Sources*, *422*, 185–195.

Jiang, N., & Xie, C. (2014). Computing and analyzing mixed equilibrium network flows with gasoline and electric vehicles. *Computer-Aided Civil and Infrastructure Engineering*, *29*(8), 626–641.

Jiang, X., & Adeli, H. (2003). Freeway work zone traffic delay and cost optimization model. *Journal of Transportation Engineering-ASCE*, *129*(3), 230–241.

Khan, Z., Khan, S. M., Chowdhury, M., Safro, I., & Ushijima-Mwesigwa, H. (2019). Wireless charging utility maximization and intersection control delay minimization framework for electric vehicles. *Computer-Aided Civil and Infrastructure Engineering*, *34*(7), 547–568.

Kliewer, N., Amberg, B., & Amberg, B. (2012). Multiple depot vehicle and crew scheduling with time windows for scheduled trips. *Public Transport*, *3*(3), 213–244.

Lam, L., & Bauer, P. (2013). Practical capacity fading model for Li-ion battery cells in electric vehicles. *IEEE Transactions on Power Electronics*, *28*(12), 5910–5918.

Lajunen, A. (2018). Lifecycle costs and charging requirements of electric buses with different charging methods. *Journal of Cleaner Production*, *172*, 56–67.

Laporte, G. (2009). Fifty years of vehicle routing. *Transportation Science*, *43*(4), 408–416.

Li, J. Q. (2014). Transit bus scheduling with limited energy. *Transportation Science*, *48*(4), 521–539.

Li, J. Q. (2016). Battery-electric transit bus developments and operations: A review. *International Journal of Sustainable Transportation*, *10*(3), 157–169.

Li, L., Lo, H. K., & Xiao, F. (2019). Mixed bus fleet scheduling under range and refueling constraints. *Transportation Research Part C: Emerging Technologies*, *104*, 443–462.

Li, M., Yin, Y., Zhang, W. B., Zhou, K., & Nakamura, H. (2011). Modeling and implementation of adaptive transit signal priority on actuated control systems. *Computer-Aided Civil and Infrastructure Engineering*, *26*(4), 270–284.

Liu, Z., Yan, Y., Qu, X., & Zhang, Y. (2013). Bus stop-skipping scheme with random travel time. *Transportation Research Part C: Emerging Technologies*, *35*, 46–56.

Logan, K. G., Nelson, J. D., & Hastings, A. (2020). Electric and hydrogen buses: Shifting from conventionally fuelled cars in the UK. *Transportation Research Part D: Transport and Environment*, *85*, 102350.

Meng, Q., & Qu, X. (2013). Bus dwell time estimation at a bus bay: A probabilistic approach. *Transportation Research Part C*, *36*, 61–71.

Millikin, M. (2019). *Number of EBs in Europe has increased from around 200 to 2,200 in 5 years*. https://www.greencarcongress.com/2019/10/20191020-busworld.html.

Montreal, G. (2018). *Montreal, Laval team up in Canada's largest order of EBs*. https://montrealgazette.com/news/local-news/montreal-laval-teamup-in-canadas-largest-order-of-electric-buses.

Naumann, M., Suhl, L., & Kramkowski, S. (2011). A stochastic programming approach for robust vehicle scheduling in public bus transport. *Procedia-Social and Behavioral Sciences*, *20*, 826–835.

Pelletier, S., Jabali, O., Mendoza, J. E., & Laporte, G. (2019). The electric bus fleet transition problem. *Transportation Research Part C: Emerging Technologies*, *109*, 174–193.

Picarelli, E., Rinaldi, M., D'Ariano, A., & Viti, F. (2020). Model and solution methods for the mixed-fleet multi-terminal bus scheduling problem. *Transportation Research Procedia*, *47*, 275–282.

Qu, X., Yu, Y., Zhou, M., Lin, C. T., & Wang, X. (2020). Jointly dampening traffic oscillations and improving energy consumption with electric, connected and automated vehicles: A reinforcement learning based approach. *Applied Energy*, *257*, 114030.

Rinaldi, M., Parisi, F., Laskaris, G., D'Ariano, A., & Viti, F. (2018). Optimal dispatching of electric and hybrid buses subject to scheduling and charging constraints. *21st IEEE International Conference on Intelligent Transportation Systems (ITSC)*, Maui, HI, USA.

Rinaldi, M., Picarelli, E., D'Ariano, A., & Viti, F. (2020). Mixed-fleet single-terminal bus scheduling problem: Modelling, solution scheme and potential applications. *Omega*, *96*, 102070.

Ritari, A., Vepsäläinen, J., Kivekäs, K., Tammi, K., & Laitinen, H. (2020). Energy consumption and lifecycle cost analysis of electric city buses with multispeed gearboxes. *Energies*, *13*(8), 2117.

Rogge, M., van der Hurk, E., Larsen, A., & Sauer, D. U. (2018). Electric bus fleet size and mix problem with optimization of charging infrastructure. *Applied Energy*, *211*, 282–295.

Schmid, V., & Ehmke, J. F. (2015). Integrated timetabling and vehicle scheduling with balanced departure times. *OR spectrum*, *37*(4), 903–928.

Shen, Y., Xu, J., & Wu, X. (2017). Vehicle scheduling based on variable trip times with expected on-time performance. *International Transactions in Operational Research*, *24*(1-2), 99–113.

Sivagnanam, A., Ayman, A., Wilbur, M., Pugliese, P., Dubey, A., & Laszka, A. (2020). Minimizing energy use of mixed-fleet public transit for fixed-route service. *arXiv*:2004.05146.

Tang, X., Lin, X., & He, F. (2019). Robust scheduling strategies of electric buses under stochastic traffic conditions. *Transportation Research Part C: Emerging Technologies*, *105*, 163–182.

Teng, J., Chen, T., & Fan, W. D. (2020). Integrated approach to vehicle scheduling and bus timetabling for an electric bus line. *Journal of Transportation Engineering, Part A: Systems*, *146*(2), 04019073.

Teoh, L. E., Khoo, H. L., Goh, S. Y., & Chong, L. M. (2018). Scenario-based electric bus operation: A case study of Putrajaya, Malaysia. *International Journal of Transportation Science and Technology*, *7*(1), 10–25.

van Kooten Niekerk, M. E., van den Akker, J., & Hoogeveen, J. (2017). Scheduling electric vehicles. *Public Transport*, *9*(1-2), 155–176.

Wang, H., & Shen, J. (2007). Heuristic approaches for solving transit vehicle scheduling problem with route and fueling time constraints. *Applied Mathematics and Computation*, *190*(2), 1237–1249.

Wang, J., Kang, L., & Liu, Y. (2019). Effects of working temperature on route planning for electric bus fleets based on dynamic programming. *Chemical Engineering Transactions*, *76*, 907–912.

Wang, J., Kang, L., & Liu, Y. (2020). Optimal scheduling for electric bus fleets based on dynamic programming approach by

considering battery capacity fade. *Renewable and Sustainable Energy Reviews*, *130*, 109978.

Wang, S., Wei, Z., Bie, Y., Wang, K., & Diabat, A. (2019). Mixed-integer second-order cone programming model for bus route clustering problem. *Transportation Research Part C: Emerging Technologies*, *102*, 351–369.

Wang, S., Zhang, W., & Qu, X. (2018). Trial-and-error train fare design scheme for addressing boarding/alighting congestion at CBD stations. *Transportation Research Part B*, *118*, 318–335

Weekes, S. (2020). *Gothenburg boosts sustainable public transport push with e-bus roll-out.* https://www.smartcitiesworld.net/news/news/gothenburg-boosts-sustainable-transpo-rt-push-with-e-bus-roll-out-4946.

Wen, M., Linde, E., Ropke, S., Mirchandani, P., & Larsen, A. (2016). An adaptive large neighborhood search heuristic for the electric vehicle scheduling problem. *Computers & Operations Research*, *76*, 73–83.

Xie, C., & Jiang, N. (2016). Relay requirement and traffic assignment of electric vehicles. *Computer-Aided Civil and Infrastructure Engineering*, *31*(8), 580–598.

Xu, Y., Zheng, Y., & Yang, Y. (2021). On the movement simulations of electric vehicles: A behavioral model-based approach. *Applied Energy*, *283*, 116356.

Yang, Z., Yu, B., & Cheng, C. (2007). A parallel ant colony algorithm for bus network optimization. *Computer-Aided Civil and Infrastructure Engineering*, *22*(1), 44–55.

Yao, E., Liu, T., Lu, T., & Yang, Y. (2020). Optimization of electric vehicle scheduling with multiple vehicle types in public transport. *Sustainable Cities and Society*, *52*, 101862.

Yu, B., Wang, H., Shan, W., & Yao, B. (2018). Prediction of bus travel time using random forests based on near neighbors. *Computer-Aided Civil and Infrastructure Engineering*, *33*(4), 333–350.

Zeng, Q., Wang, M., Shen, L., & Song, H. (2019). Sequential scheduling method for FJSP with multi-objective under mixed work calendars. *Processes*, *7*(12), 888.

Zhang, X., Rey, D., & Waller, S. T. (2018). Multitype recharge facility location for electric vehicles. *Computer-Aided Civil and Infrastructure Engineering*, *33*(11), 943–965.

Zhang, L., Zeng, Z., & Qu, X. (2020). On the role of battery capacity fading mechanism in the lifecycle cost of electric bus fleet. *IEEE Transactions on Intelligent Transportation Systems*, 1–10.doi: 10.1109/TITS.2020.3014097.

Zhao, X., Ye, Y., Ma, J., Shi, P., & Chen, H. (2020). Construction of electric vehicle driving cycle for studying electric vehicle energy consumption and equivalent emissions. *Environmental Science and Pollution Research International*, *27*(30), 37395–37409.

Zhao, X., Zhao, X., Yu, Q., Ye, Y., & Yu, M. (2020). Development of a representative urban driving cycle construction methodology for electric vehicles: A case study in Xi'an. *Transportation research. Part D, Transport and environment*, *81*, 102279.

Zhao, D., Li, X., & Cui, J. (2019). A simulation-based optimization model for infrastructure planning for electric autonomous vehicle sharing. *Computer-Aided Civil and Infrastructure Engineering*, 1–19.Retrieved from https://doi.org/10.1111/mice.12506.

Zhou, G. J., Xie, D. F., Zhao, X. M., & Lu, C. (2020). Collaborative optimization of vehicle and charging scheduling for a bus fleet mixed with electric and traditional buses. *IEEE Access*, *8*, 8056–8072.

APPENDIX A

Energy consumption probability distribution function

After collecting historical operation data of electric buses (EBs), the parameters of each bus on each trip are organized as one row, including actual energy consumption, actual trip travel time, battery state of charge (SOC) at departure time, and average hourly temperature.

Step 1: Based on Section 2.1.3, the linear regression model for the actual energy consumption is formulated as follows:

$$w_\ell^- = \beta_1 soc_\ell^d + \beta_2 t_\ell + \beta_3 \bar{T}_\ell^0 + \beta_0 + \varepsilon_\ell \quad \text{(A-1)}$$

where w_ℓ^- is the actual energy consumption of the l-th sample, kWh; soc_ℓ^d is the l-th battery SOC at departure time, %; t_ℓ is the l-th actual trip travel time, min; $\bar{T}^0$ is the l-th average hourly temperature, °F; ε_ℓ is the stochastic error term; $\beta_1, \beta_2, \beta_3$, and β_0 are regression parameters; ℓ is the sample serial number, $1 \le \ell \le \Lambda$; and Λ is the number of samples.

Step 2: Use the ordinary least square method (OLS) to conduct parameter fitting for the multiple linear regression model. The estimated regression model is

$$w_\ell^- = \hat{w}_\ell^- + \hat{\varepsilon}_\ell \quad \text{(A-2)}$$

where $\hat{\varepsilon}_\ell$ is the residual error of the linear regression model; $\hat{w}_\ell^-$ is the fitted value of energy consumption of the EB, which satisfies

$$\hat{w}_\ell^- = \hat{\beta}_1 soc_\ell^d + \hat{\beta}_2 t_\ell + \hat{\beta}_3 \bar{T}_\ell^0 + \hat{\beta}_0 \quad \text{(A-3)}$$

The loss function is as follows:

$$\Phi = \sum_{\ell=1}^{\Lambda} (\hat{\varepsilon}_\ell)^2 = \sum_{\ell=1}^{\Lambda} \left[w_\ell^- - \left(\hat{\beta}_1 soc_\ell^d + \hat{\beta}_2 t_\ell + \hat{\beta}_3 \bar{T}_\ell^0 + \hat{\beta}_0 \right) \right]^2$$

$$\text{(A-4)}$$

Based on OLS, to minimize the loss function, $\frac{\partial \Phi}{\partial \hat{\beta}_1} = 0$, $\frac{\partial \Phi}{\partial \hat{\beta}_2} = 0$, $\frac{\partial \Phi}{\partial \hat{\beta}_3} = 0$, and $\frac{\partial \Phi}{\partial \hat{\beta}_0} = 0$ should be satisfied. $\hat{\beta}_1$, $\hat{\beta}_2$, $\hat{\beta}_3$ and $\hat{\beta}_0$ can be obtained by solving this system of linear algebraic equations. Then, the coefficient of determination R^2 is applied to evaluate the goodness of fit of observed

values. The closer the R^2 is to 1, the better the observed values match the model.

Step 3: Utilize the White test to determine whether the heteroscedasticity exists. With the square of the aforementioned residual error $\hat{\varepsilon}_\ell^2$ as the explained variable, the combinations of the standard term, square term, and cross term of each explaining variables in the regression model as explaining variables, the auxiliary regression model is built as follows:

$$\hat{\varepsilon}_\ell^2 = \zeta_0 + \zeta_1 soc_\ell^d + \zeta_2 t_\ell + \zeta_3 \bar{T}_\ell^0 + \zeta_4 \left(soc_\ell^d\right)^2 + \zeta_5 (t_\ell)^2$$
$$+ \zeta_6 \left(\bar{T}_\ell^0\right)^2 + \zeta_7 soc_\ell^d t_\ell + \zeta_8 t_\ell \bar{T}_\ell^0 + \zeta_9 soc_\ell^d \bar{T}_\ell^0 + \xi_\ell$$
$$\text{(A-5)}$$

Under the hypothesis of the homoscedasticity H_0: $\zeta_1 = \zeta_2 = \zeta_3 = \zeta_4 = \zeta_5 = \zeta_6 = \zeta_7 = \zeta_8 = \zeta_9$, the parameter estimation of the auxiliary regression model is conducted using OLS to obtain the corresponding R^2. Under the considered significance level α, if $\Lambda R^2 \leq \chi_\alpha^2(9)$ is satisfied, the null hypothesis is accepted that there does not exist heteroscedasticity and goes to step 4; otherwise, it is accepted that heteroscedasticity exists and goes to step 5.

Step 4: If there does not exist heteroscedasticity, the probabilities of ε_ℓ and w_ℓ^- are assumed to follow the normal distribution. Based on the hypothesis of OLS $\varepsilon_\ell \sim N(0, \hat{\sigma}^2)$, w_ℓ^- also complies with the following normal distribution:

$$w_\ell^- \sim N\left(\hat{\beta}_1 soc_\ell^d + \hat{\beta}_2 t_\ell + \hat{\beta}_3 \bar{T}_\ell^0 + \hat{\beta}_0, \hat{\sigma}^2\right) \quad \text{(A-6)}$$

where $\hat{\sigma}^2$ is the estimation of σ^2, which can be calculated by the following equation:

$$\hat{\sigma}^2 = \frac{\sum_{\ell=1}^{\Lambda} \left(w_\ell^- - \hat{\beta}_1 soc_\ell^d + \hat{\beta}_2 t_\ell + \hat{\beta}_3 \bar{T}_\ell^0 + \hat{\beta}_0\right)^2}{\Lambda - 4} \quad \text{(A-7)}$$

Step 5: If the heteroscedasticity exists, apply the weighted least square (WLS) method and formulate a new model without heteroscedasticity. For ε_ℓ satisfies $\text{Var}(\varepsilon_\ell) \approx \hat{\varepsilon}_\ell^2$ approximately, $\frac{1}{\sqrt{\hat{\varepsilon}_\ell^2}} = \frac{1}{|\hat{\varepsilon}_\ell|}$ is used as the weight and to multiply both sides of the original model. The following model is obtained as follows:

$$\frac{1}{|\hat{\varepsilon}_\ell|} w_\ell^- = \beta_1 \frac{1}{|\hat{\varepsilon}_\ell|} soc_\ell^d + \beta_2 \frac{1}{|\hat{\varepsilon}_\ell|} t_\ell + \beta_3 \frac{1}{|\hat{\varepsilon}_\ell|} \bar{T}_\ell^0 + \beta_0 \frac{1}{|\hat{\varepsilon}_\ell|} + \frac{1}{|\hat{\varepsilon}_\ell|} \varepsilon_\ell$$
$$\text{(A-8)}$$

$$\text{Var}\left(\frac{1}{|\hat{\varepsilon}_\ell|} \varepsilon_\ell\right) = \left(\frac{1}{|\hat{\varepsilon}_\ell|}\right)^2 \text{Var}(\varepsilon_\ell) = \frac{1}{\hat{\varepsilon}_\ell^2} \hat{\varepsilon}_\ell^2 = 1 \quad \text{(A-9)}$$

The WLS method has been widely used in the field of statistics to tackle the issue of heteroscedasticity. The main principle of the method is to assign different weights to different observation points. The method tends to balance the regression model by using weights that are inversely proportional to the squares of residuals of the explanatory variables to reduce the impacts of unprecise observations on parameter estimates so as to overcome heteroscedasticity.

The current new model satisfies the homoscedasticity. The modified estimation regression model for energy consumption is obtained as follows:

$$\hat{w}_\ell^- = \hat{\beta}_1' soc_\ell^d + \hat{\beta}_2' t_\ell + \hat{\beta}_3' \bar{T}_\ell^0 + \hat{\beta}_0' \quad \text{(A-10)}$$

where $w_\ell^- \sim N(\hat{w}_\ell^-, 1)$. Therefore, under certain values of independent variables, the probability density function of energy consumption is

$$f\left(w^- \middle| soc^d = soc^{d,g}, t = t^g, \bar{T}^0 = \bar{T}^{0,g}\right) = \frac{1}{\sqrt{2\pi}} e^{-\frac{(w^- - \hat{w}^-)^2}{2}}$$
$$\text{(A-11)}$$

APPENDIX B
Scheduled departure timetable of route 108

No.	Time	No.	Time	No.	Time	No.	Time	No.	Time	No.	Time	No.	Time	No.	Time	No.	Time	No.	Time
1	5:30 a.m.	12	7:25 a.m.	23	8:20 a.m.	34	9:36 a.m.	45	11:40 a.m.	56	1:08 p.m.	67	3:06 p.m.	78	4:55 p.m.	89	6:01 p.m.	100	7:25 p.m.
2	5:45 a.m.	13	7:30 a.m.	24	8:25 a.m.	35	9:48 a.m.	46	11:48 a.m.	57	1:16 p.m.	68	3:17 p.m.	79	5:01 p.m.	90	6:07 p.m.	101	7:40 p.m.
3	6:00 a.m.	14	7:35 a.m.	25	8:30 a.m.	36	10:00 a.m.	47	11:56 a.m.	58	1:27 p.m.	69	3:28 p.m.	80	5:07 p.m.	91	6:13 p.m.	102	7:55 p.m.
4	6:15 a.m.	15	7:40 a.m.	26	8:35 a.m.	37	10:12 a.m.	48	12:04 p.m.	59	1:38 p.m.	70	3:39 p.m.	81	5:13 p.m.	92	6:19 p.m.	103	8:10 p.m.
5	6:30 a.m.	16	7:45 a.m.	27	8:40 a.m.	38	10:24 a.m.	49	12:12 p.m.	60	1:49 p.m.	71	3:50 p.m.	82	5:19 p.m.	93	6:25 p.m.	104	8:25 p.m.
6	6:45 a.m.	17	7:50 a.m.	28	8:45 a.m.	39	10:36 a.m.	50	12:20 p.m.	61	2:00 p.m.	72	4:01 p.m.	83	5:25 p.m.	94	6:31 p.m.	105	8:40 p.m.
7	6:55 a.m.	18	7:55 a.m.	29	8:50 a.m.	40	10:48 a.m.	51	12:28 p.m.	62	2:11 p.m.	73	4:12 p.m.	84	5:31 p.m.	95	6:37 p.m.	106	8:55 p.m.
8	7:05 a.m.	19	8:00 a.m.	30	8:55 a.m.	41	11:00 a.m.	52	12:36 p.m.	63	2:22 p.m.	74	4:23 p.m.	85	5:37 p.m.	96	6:43 p.m.	107	9:10 p.m.
9	7:10 a.m.	20	8:05 a.m.	31	9:03 a.m.	42	11:12 a.m.	53	12:44 p.m.	64	2:33 p.m.	75	4:33 p.m.	86	5:43 p.m.	97	6:49 p.m.	108	9:25 p.m.
10	7:15 a.m.	21	8:10 a.m.	32	9:12 a.m.	43	11:22 a.m.	54	12:52 p.m.	65	2:44 p.m.	76	4:43 p.m.	87	5:49 p.m.	98	6:59 p.m.	109	9:40 p.m.
11	7:20 a.m.	22	8:15 a.m.	33	9:24 a.m.	44	11:32 a.m.	55	1:00 p.m.	66	2:55 p.m.	77	4:49 p.m.	88	5:55 p.m.	99	6:10 p.m.	110	9:55 p.m.